Energy Technology
Generation, Conversion, Storage, Distribution
www.entechnol.de

Check for updates

Micro versus Nano: Impact of Particle Size on the Flow Characteristics of Silicon Anode Slurries

*Rassmus Andersson, Guiomar Hernández, Kristina Edström, and Jonas Mindemark**

Silicon is interesting for use as a negative electrode material in Li-ion batteries due to its extremely high gravimetric capacity compared with today's state-of-the-art material, graphite. However, during cycling the Si particles suffer from large volume changes, leading to particle cracking, electrolyte decompositions, and electrode disintegration. Although utilizing nm-sized particles can mitigate some of these issues, it would instead be more cost-effective to incorporate µm-sized silicon particles in the anode. Herein, it is shown that the size of the Si particles not only influences the electrode cycling properties but also has a decisive impact on the processing characteristics during electrode preparation. In water-based slurries and suspensions containing µm-Si and nm-Si particles, the smaller particles consistently give higher viscosities and more pronounced viscoelastic properties, particularly at low shear rates. This difference is observed even when the Si particles are present as a minor component in blends with graphite. It is found that the viscosity follows the particle volume fraction divided by the particle radius, suggesting that it is dependent on the surface area concentration of the Si particles.

1. Introduction

Silicon has recently received great attention as a material to replace graphite in the negative electrodes in Li-ion batteries due to the virtue of its extremely high gravimetric capacity of 3579 mAh g^{-1} at room temperature.[1–3] With about ten times higher capacity than graphite (372 mAh g^{-1}),[3–5] Si has the possibility to help satisfying our increasing demand for high-capacity energy storage by improving the energy density of the negative electrode in Li-ion batteries. This higher capacity, however, comes at a high penalty of significant volume expansion of up to 400% at elevated temperature during lithiation when Li is inserted into Si to form the crystalline phase $Li_{22}Si_5$, which results in cracking and disintegrating of the electrode particles and ultimately loss of capacity.[3–8] Depending on the particle size of the Si, this problem is more or less pronounced. In general, the decomposition of Si electrodes is most severe for larger particles in the µm-range, whereas smaller particles below a certain size in the nm-range exhibit less cracks or fractures upon continued cycling.[4,9–12] For utilization of µm-sized Si, the best approach appears to be combining it with graphite in composite electrodes.[13,14] Despite this fact, there are studies reporting successfully cycled electrodes with µm-sized Si particle. Cheng and co-workers used a combination of different carbon materials to improve the interparticle network in the electrode,[15] whereas Bao and co-workers used a stretchable and self-healing polymer to reconnect particles after cycling[16] and Chen and co-workers incorporated nm-sized Si into larger µm-sized particles[17] to improve the cycle life of the electrode. From an economical point of view, of course, it would be rather optimal to realize the use of the larger and cheaper µm-sized Si particles.

Replacing graphite with Si in Li-ion battery anodes does not only affect the cycling properties but also the processing of the particles into useful electrodes. Compared with graphite, which has a layered structure of covalently bonded carbons in 2D sheets with weak van der Waals interactions between the sheets, crystalline Si has a diamond structure consisting of a 3D network of covalently bonded Si. This gives graphite the particle shape appearance of flat flakes, whereas the Si particles attain spherical shapes. The particles also have different surface chemistries and are therefore often processed using different binder and solvent systems. For graphite, until the early 2000s, organic solvents were commonly used because of the hydrophobicity of graphite, whereas water-based systems are preferred for Si because of its native surface oxide layer.[18] For environmental and occupational safety reasons, the more benign water-based processing is naturally preferred and water has nowadays become the standard solvent for both materials.[18] A good candidate for water-based processing of both graphite and Si is the mixed binder system consisting of sodium carboxymethyl cellulose (Na-CMC) and styrene–butadiene rubber (SBR), which also is a preferred system for Si.[8,11,19–21] This system works for both graphite and Si, as it can be designed to be more or less hydrophilic, depending on the degree of substitution of functional groups, i.e., amount of hydroxyl groups replaced with carboxyl groups in the structure.

R. Andersson, Dr. G. Hernández, Prof. K. Edström, Dr. J. Mindemark
Department of Chemistry – Ångström Laboratory
Uppsala University
Box 538, Uppsala SE-751 21, Sweden
E-mail: jonas.mindemark@kemi.uu.se

The ORCID identification number(s) for the author(s) of this article can be found under https://doi.org/10.1002/ente.202000056.

© 2020 The Authors. Published by WILEY-VCH Verlag GmbH & Co. KGaA, Weinheim. This is an open access article under the terms of the Creative Commons Attribution-NonCommercial License, which permits use, distribution and reproduction in any medium, provided the original work is properly cited and is not used for commercial purposes.

DOI: 10.1002/ente.202000056

When graphite is used, it will interact with the backbone of the CMC and the functional groups in Na-CMC will dissociate and stabilize the suspension, whereas when Si is used, an esterification reaction will occur between the Na-CMC and the silicon oxide on the Si surface, creating strong covalent bonds.[18,19]

Electrodes for Li-ion batteries are manufactured by coating a thick slurry containing the active material particles onto metal foil. During this process, the slurry is subjected to shear rates typically in the order of $100\,s^{-1}$. Depending on the rheological characteristics of the slurry, the resulting shear stress can differ substantially. The flow characteristics will also affect how the slurry settles post-application. This will have a decisive impact on the quality of the electrode coatings and the resulting performance of the battery, as an inhomogeneous distribution of the particles in the coating possibly can result in isolated active material particles in the final electrode. During cycling, an inhomogeneous particle distribution can create high tensions and stress the electrode in parts with high loadings, which are then more prone to failure.[20,22]

This article investigates the flow characteristics of water-based Si-containing slurries, revealing that changing the Si particle size not only affects the cycling characteristics but also completely changes the processing properties during manufacturing of the electrodes. This is found to be the case also when the Si particle are only present as a minor component together with graphite.

2. Results and Discussion

A viable solution to enable the use of Si as a functional anode material is to incorporate it as a high-capacity additive together with graphite. By replacing about 10 wt% of the graphite with Si, the electrode may acquire an increased capacity from the Si while retaining the stability of the graphite anode.[13,23,24] We prepared graphite/Si slurries using two different kinds of Si particles primarily characterized by disctinctly different sizes, as shown in **Figure 1**.

The surface area of the particles was determined using N_2 physisorption experiments (Figure S1, Supporting Information) to $45.22\,m^2\,g^{-1}$ for nm-Si and $4.10\,m^2\,g^{-1}$ for μm-Si. Assuming that the particles are spherical, this amounts to an average particle radius of 29 nm for the nm-Si and 315 nm for the μm-Si particles. Considering the morphologies of the particles in the scanning electron microscopy (SEM) images in Figure 1, this assumption is clearly more valid for the nm-Si particles, but still serves as a useful measure of comparison of the different sizes. It should, however, be noted that this is an average size measure of all particles and particle dimensions based solely on the surface area of the particles. After slurry processing, the particle sizes were again assessed by means of SEM, to evaluate whether the ball milling led to a reduction in particle size.[25] The SEM images in **Figure 2** confirm consistent particle sizes, with large μm-Si particles up to 4 μm retained in the final electrodes.

While preparing slurries of the nm- and μm-size Si as a minor component (10 wt%) of the active material together with graphite, we noted that the slurries displayed markedly different handling characteristics. The effects of the different particle sizes are immediately noticeable upon visual inspection as the slurry containing μm-sized Si particles flows like a liquid, whereas the slurry containing nm-sized Si instead shows clear viscoelastic tendencies (Figure S2, Supporting Information).

The ideal slurry shows a non-Newtonian flow behavior, in the sense that it should be shear-thinning, i.e., decrease in viscosity with increasing shear rate. A high viscosity at low shear rates prevents sedimentation of the slurry particles during the drying process, whereas a low viscosity at high shear rates improves mixing during the slurry preparation.[26,27] This can also be seen by studying the yield point (cross-over) when measuring the complex modulus (G^*) described by the storage modulus (G') and the loss modulus (G''). When $G' > G''$, the response of the slurry will appear elastic and when $G' < G''$, the response will be predominantly viscous. In general, a greater G'' than G' immediately after casting helps the leveling of the slurry coating, which promotes an even mass loading over the whole electrode. Yet, a more elastic behavior is desired as it preserves a sharp coating edge and prevents settling of the slurry after casting.[20,27,28]

As shown in **Figure 3**a, slurries containing nm- as well as μm-sized Si particles are showing elements of viscoelastic behavior with a phase angle (δ) between the applied strain and resulting stress being in the interval $0° < \delta < 90°$, where $\delta = 0°$ representing a purely elastic and $\delta = 90°$ a purely viscous response. The phase angle is related to G' and G'' according to $\tan\delta = \frac{G''}{G'}$.[29,30] Figure S3, Supporting Information, shows that the linear viscoelastic region extends up to about 10% strain for these samples.

Notable differences in the viscoelastic response for the two slurries can be noted in Figure 3a. For the μm-Si slurry, G'' is larger than G' over the whole frequency interval, indicating a predominantly viscous and liquid-like behavior. This separates

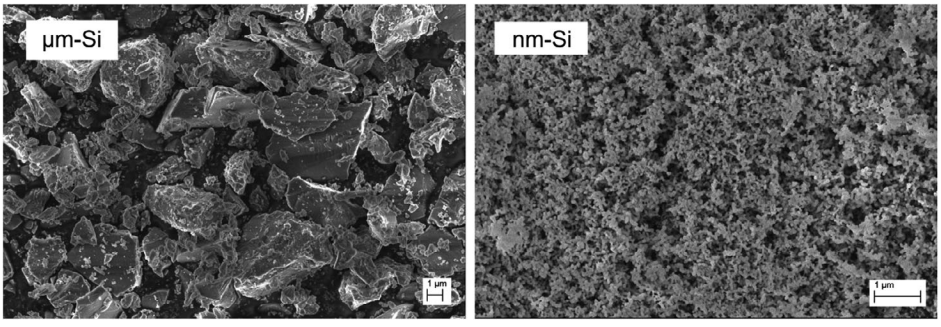

Figure 1. SEM images of the pristine μm-Si and nm-Si particles.

© 2020 The Authors. Published by WILEY-VCH Verlag GmbH & Co. KGaA, Weinheim

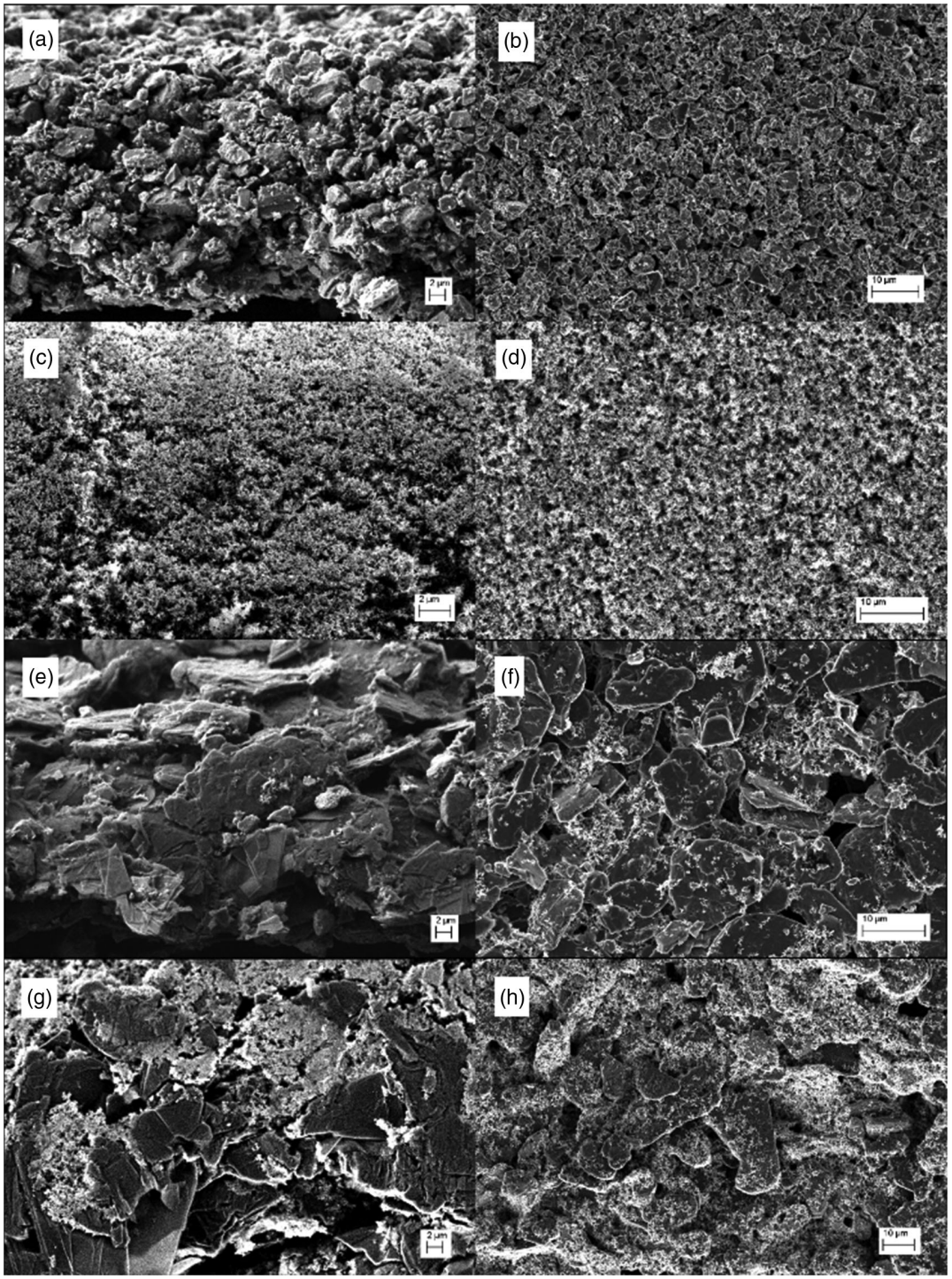

Figure 2. SEM images of Si/graphite composite electrodes. a) µm-Si, cross-sectional view; b) µm-Si, top view; c) nm-Si, cross-sectional view; d) nm-Si, top view; e) µm-Si/graphite composite, cross-sectional view; f) µm-Si/graphite composite, top view; g) nm-Si composite, cross-sectional view, h) nm-Si composite, top view. The slurry composition was: active material:Na-CMC:SBR:CB in the ratio 9.3:83.7:3.3:1.7:2 by weight. For the composite, the ratio Si:graphite was 1:9 by weight.

it from the nm-Si slurry, which has a more distinct elastic response, particularly at low frequencies, which is reminiscent of that of a typical gel.[30,31] As these slurries are identical but for the Si particles, this remarkable difference in flow behavior can be directly attributed to the size of the particles, even though the Si is only present as a minor component (3.3 wt% of the slurry). This minor difference is also visible in Figure 3b, where both Si-containing slurries display shear-thinning effects with

© 2020 The Authors. Published by WILEY-VCH Verlag GmbH & Co. KGaA, Weinheim

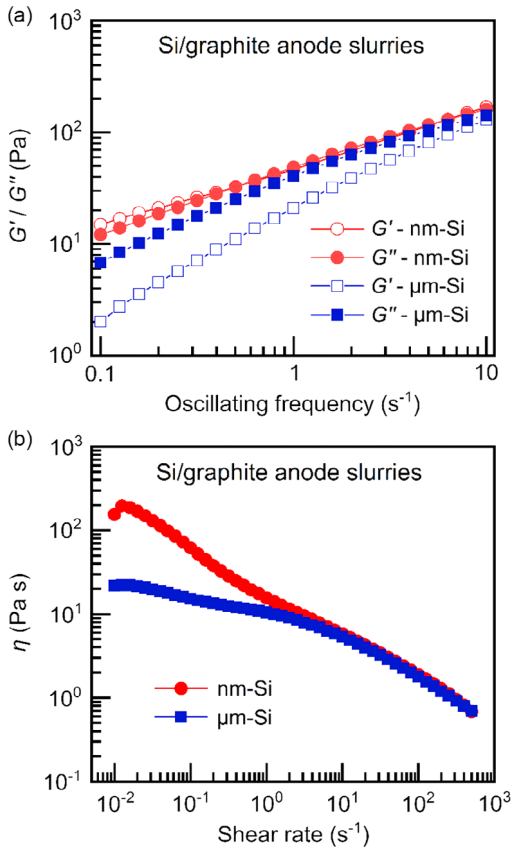

Figure 3. a) Oscillating frequency sweep and b) rotational viscometry measurements of slurries containing 35 wt% solid materials and 65 wt% water. The solid material composition was Si:graphite:Na-CMC:SBR:CB in a ratio of 9.3:83.7:3.3:1.7:2 by weight.

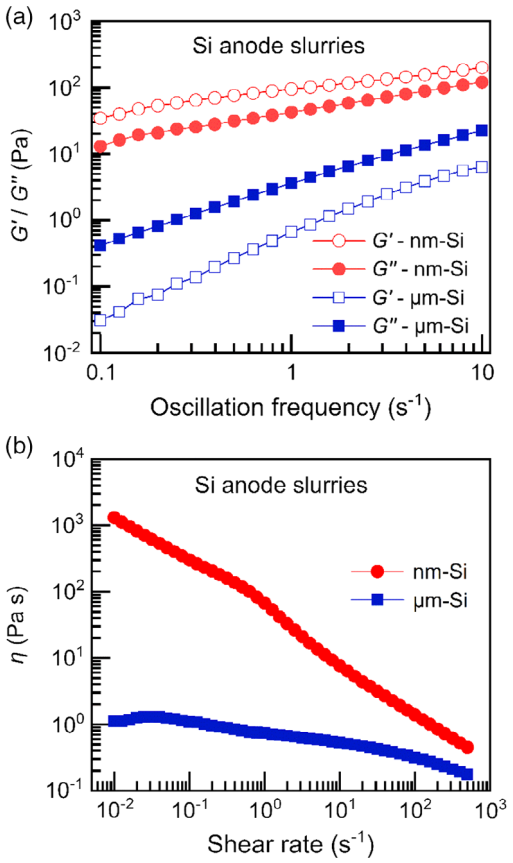

Figure 4. a) Oscillating frequency sweep and b) rotational viscometry measurements on slurries containing 13.5 wt% solid content in water. The solid material composition was Si, CB, and Na-CMC in a ratio of 80:12:8 by weight.

increasing shear rates, i.e., a disruptive behavior, originating from breaking of the structure when the stress is increasing on the material with increasing shear rates.[32] At low shear rates, there is a clear difference between the two slurries; however, at shear rates of typical process speeds of around 100 s^{-1}, this difference diminishes and the apparent viscosities of the two slurries coincide. Thus, the flow behavior of these slurries would be nearly identical during the coating process (Figure S4a, Supporting Information), but with notable differences during subsequent steps where no external stress is applied.

As the rheological properties are so heavily influenced by the Si particle content, the rheological response naturally changes drastically as the graphite content is reduced in favor of increasing amounts of Si (Figure S5, Supporting Information). The rheological differences between the slurries become even more pronounced when the graphite is completely eliminated to give slurries with Si as the sole active material. In **Figure 4**a, the results from frequency sweeps of slurries with only Si as the active material can be seen. Now the rheological differences between the two Si materials is clear; over the entire measured frequency interval, the nm-Si slurry exhibits a predominantly elastic response, in contrary to the µm-Si slurry that exhibits a viscous response. This difference is also obvious in the viscometry measurement in Figure 4b, which shows a strong shear-thinning behavior for the nm-Si slurry, while this behavior is not nearly as pronounced for the µm-Si slurry. The slurry with the larger particles also has a markedly lower apparent viscosity throughout the measurement interval. These results clearly show how the different particle sizes give rise to slurries with completely different flow behavior. This is not least true at relevant coating speeds (Figure S4b, Supporting Information), particularly with small coating gaps.

The morphology of electrodes prepared from Si/graphite composite slurries are shown in the SEM micrographs in Figure 2. As can be seen, the particles seems to be well distributed all over the surface (top view) and within the electrode coating (cross-sectional view) for all prepared electrodes. The mass loading and coating thickness of both Si/graphite and pure Si electrodes are shown in Figure S6, Supporting Information. The density of the electrode coatings, calculated from the previous data, is shown in Figure S7, Supporting Information, and is roughly the same for all electrodes, with the exception of the pure nm-Si coatings, which experienced some mass losses during the punching process, indicating poor adhesion of the electrode coatings for these samples. The similar density of the coatings is expected as both Si and graphite have roughly the same density (2.33 and 2.26 g cm^{-3}, respectively) and is an indication of similar porosity of all electrode coatings.

© 2020 The Authors. Published by WILEY-VCH Verlag GmbH & Co. KGaA, Weinheim

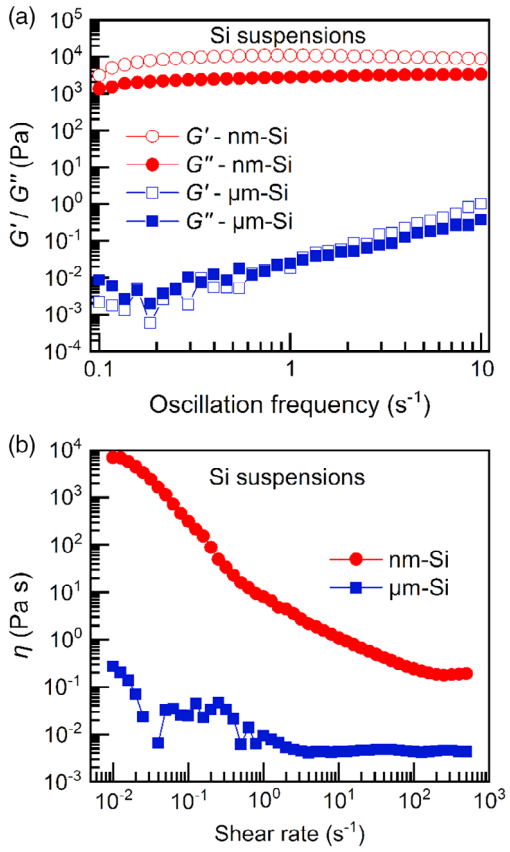

Figure 5. a) Oscillating frequency sweep and b) rotational viscometry measurements of dispersions consisting of 25 wt% silicon powder and 75 wt% water.

To further highlight that the differences in flow behavior are due to the Si particles, slurries were prepared without either graphite, carbon black (CB) or binders added, i.e., dispersions of only Si in water. In **Figure 5**a, the rheological differences between the nm-Si and µm-Si suspensions are clearly observed. In the absence of binder added as a dispersing agent, only the nm-sized Si particles managed to form a stable suspension other than at high shear rates. This can be noted as low moduli and instabilities in the rheological response at low shear rates for the µm-Si slurry. In contrast, the nm-Si slurry displays a very high and dominating G' over the entire measured frequency interval. Remarkably, the G' (and the G'') for the nm-Si suspension is almost constant over the entire frequency interval, i.e., it is frequency-independent with a phase angle δ close to 0°, which is a typical response for a solid material.[30] Such behavior is known for suspensions with high particle concentrations, where particle–particle interactions are present. In these suspensions, the particles tend to be unevenly distributed and aggregate and flocculation of particles might be present.[32]

Even if the response for the µm-Si suspension displays instabilities at low shear rates (where the resulting shear stress is extremely low), the contrast between the two suspensions in Figure 5 is striking considering that they have identical mass loadings (and volume fractions) of Si particles, with size being the main difference. Even when considering a wider range of

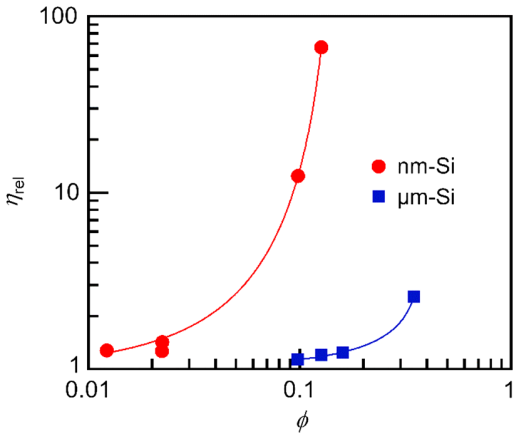

Figure 6. Plot of the relative viscosity η_{rel} at different volume fractions ϕ of particles for µm-Si and nm-Si particle suspensions at a shear rate of 100 s^{-1}. The solid lines represent fits to the Krieger–Dougherty model ($\phi_{max} = 0.16$, $K = 2.58$ for nm-Si; $\phi_{max} = 0.38$, $K = 0.41$ for µm-Si).

particle concentrations, the contrast between the different particle sizes is clear. **Figure 6** compares the relative viscosity η_{rel} (defined as the suspension viscosity divided by the viscosity of the pure solvent) at a shear rate of 100 s^{-1} for nm- and µm-Si particle suspensions at a range of volume fractions ϕ, showing clearly how the different particle sizes appear as two distinct series.

The flow behavior of suspensions of hard spheres at high concentrations ($\phi > 0.05$) can be described using the Krieger–Dougherty model[30,33,34]

$$\eta_{rel} = \left(1 - \frac{\phi}{\phi_{max}}\right)^{-K\phi_{max}} \quad (1)$$

where ϕ_{max} is the maximum solid loading and K is a constant that is equal to 2.5 for monodispersed spherical particles. As is evident from Figure 6, this model well describes the Si suspension viscosity data. However, it is clear that the different particles fall onto two separate curves; for both particle sizes taken together, the viscosity scales poorly with ϕ. Instead, we find that the viscosity of these slurries scales much better with ϕ/r, where r is the

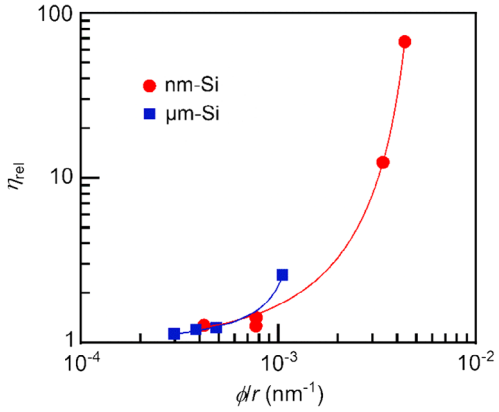

Figure 7. Plot of the relative viscosity η_{rel} versus ϕ/r of particles for µm-Si and nm-Si particle suspensions at a shear rate of 100 s^{-1}.

© 2020 The Authors. Published by WILEY-VCH Verlag GmbH & Co. KGaA, Weinheim

particle radius as calculated from the surface area measurements presented earlier. The measure ϕ/r is proportional to the particle surface area per unit volume (for the mathematical derivation, please refer to the Supporting Information) and as shown in **Figure 7**, when plotted as a function of ϕ/r, the viscosity data for both series approximately fall onto a single master curve. In contrast, when η_{rel} is plotted against ϕ/r^3 (proportional to the particle concentration), we find similarly poor correlation as for the particle volume fraction with the two particle sizes again appearing as two distinct series (Figure S8, Supporting Information). This indicates that the particle surface area is a key variable for describing and predicting the flow behavior of Si-containing electrode slurries.

3. Conclusion

Although incorporation of Si boosts the capacity of negative electrodes in Li-ion batteries, the size of the Si particles has a decisive impact not only on the electrochemical performance but also on the processing characteristics of Si-containing negative electrode slurries during electrode manufacturing. Pronounced differences in rheological response were observed between slurries containing either μm-sized or nm-sized Si particles, where the nm-sized Si particles led to a predominantly elastic behavior, whereas the μm-Si-containing slurries displayed more distinctly viscous behavior. This difference was retained even when Si was only added as a minor component in a graphite matrix.

By assuming the behavior of hard spheres, described by the Krieger–Dougherty model, a good correlation was achieved with the experimental results for suspensions consisting solely of Si particles in water. However, poor correlation was observed between the relative viscosity of the particle suspensions and either the particle concentration or volume fraction of particles. Instead, it was seen that the relative viscosity correlates much better with the surface area concentration of the particles in suspension. The surface area of Si particles may thus be an important parameter for predicting and controlling slurry rheology in electrode manufacturing.

4. Experimental Section

Materials: μm-sized Si powder (Silgrain e-Si 400, D50 = 3.1 μm) from ELKEM, nm-sized Si powder (crystalline, APS < 50 nm, 98%, laser synthesized from vapor phase, surface area 70–100 $m^2 g^{-1}$) from Alfa Aesar, graphite powder (SLP30, particle size <30 μm) from Timcal Timrex, CB Super C65 (particle size 150 nm) from Timcal C-Nergy, Na-CMC; Walocel CRT 2000 Pa, DS: 0.89 from DOW and SBR, PSBR100, dispersed in water, 15 ± 0.5% solid content from Targray were all used as received. Deionized water was used as the solvent and suspension medium.

Slurry Preparation: First, the slurries were prepared by mixing the Si, graphite, CB, and Na-CMC in a 50 mL ceramic ball-mill jar. Two larger and two smaller ceramic balls with a diameter of about 19 and 12 mm, respectively, were added to the jar, before finally adding SBR and deionized water. The total weight of the components in the ball mill was about 6 mg (≈6 mL). The amount and ratios of the solid components in each slurry where varied and are stated when appropriate. The slurries were mechanically mixed for 1–1.5 h in a Retsch planetary ball mill with a rotational speed of 300 rpm before performing the rheological measurements. The Si suspensions were prepared with the same procedure as the slurries.

Electrode Preparation: The electrodes were prepared by casting the slurries on a copper foil with a thickness of about 22 μm by a doctor blade with coating gap of 100 and 200 μm. The coating speed was about 0.012 m s^{-1}. The coating was thereafter dried at ambient temperature for 24 h, before 13 mm electrode discs were punched out and finally dried at 80 °C in vacuum for 12 h.

Rheological Measurements: The rheological analysis of the samples was performed with a TA Instruments AR2000. For the measurements, a 2°, 40 mm diameter stainless-steel cone geometry was used. The measurements were performed at 25 °C in air, with a solvent trap keeping an atmosphere of saturated humidity to prevent evaporation from the samples.

All samples were first subjected to a frequency sweep with a controlled strain of 1% in the frequency interval 0.1–10 Hz. Thereafter, a steady-state flow experiment was performed with a pre-shear conditioning step of 1 s^{-1} for 1 min, to mimic the initial disruptive breakdown of the structure in the slurry during the coating process of an electrode. During the steady-state flow step, the shear rate was controlled in an interval from 0.01 to 500 s^{-1} and then back from 500 s^{-1} down to 0.01 s^{-1}.

An amplitude test was performed on the Si/graphite composite slurries with an oscillating shear stress sweep between 0.01 and 1000 Pa at the frequency 1 Hz; the results are shown in Figure S3, Supporting Information.

Scanning Electron Microscopy: A Carl Zeiss Merlin SEM with an acceleration voltage of 3–5 kV and a beam current of 100 pA was used to analyze the particles and the electrode coating morphologies, the particle distributions, and particle sizes. Both the surface and the cross-section of the electrodes were analyzed. The cross-sectional samples were prepared by slicing the samples with a rotary cutter and were assembled on a holder with a 90° angle.

N_2 Physisorption: N_2 physisorption measurements were performed on an ASAP2020 (Micromeritics). The measurement was carried out at the boiling temperature of the adsorbate gas (nitrogen), i.e., at 77 K (−196 °C).

Supporting Information

Supporting Information is available from the Wiley Online Library or from the author.

Acknowledgements

The authors acknowledge STandUP for Energy and the Swedish Energy Agency (grant agreement no. 40466-1, project "SiLiCoat").

Conflict of Interest

The authors declare no conflict of interest.

Keywords

electrode materials, Li-ion batteries, silicon anode slurries

Received: January 14, 2020
Revised: April 9, 2020
Published online: May 10, 2020

[1] N. Nitta, F. Wu, J. T. Lee, G. Yushin, *Mater. Today* **2015**, *18*, 252.
[2] B. Key, R. Bhattacharyya, M. Morcrette, V. Seznec, J. M. Tarascon, C. P. Grey, *J. Am. Chem. Soc.* **2009**, *131*, 9239.
[3] B. Liang, Y. Liu, Y. Xu, *J. Power Sources* **2014**, *267*, 469.

© 2020 The Authors. Published by WILEY-VCH Verlag GmbH & Co. KGaA, Weinheim

[4] U. Kasavajjula, C. Wang, A. J. Appleby, *J. Power Sources* **2007**, *163*, 1003.
[5] N. Nitta, G. Yushin, *Part. Part. Syst. Charact.* **2014**, *31*, 317.
[6] A. Casimir, H. Zhang, O. Ogoke, J. C. Amine, J. Lu, G. Wu, *Nano Energy* **2016**, *27*, 359.
[7] B. P. N. Nguyen, S. Chazelle, M. Cerbelaud, W. Porcher, B. Lestriez, *J. Power Sources* **2014**, *262*, 112.
[8] A. Tranchot, H. Idrissi, P. X. Thivel, L. Roué, *J. Power Sources* **2016**, *330*, 253.
[9] J. Xiao, W. Xu, D. Wang, D. Choi, W. Wang, X. Li, G. L. Graff, J. Liu, J.-G. Zhang, *J. Electrochem. Soc.* **2010**, *157*, A1047.
[10] X. H. Liu, L. Zhong, S. Huang, S. X. Mao, T. Zhu, J. Y. Huang, *ACS Nano* **2012**, *6*, 1522.
[11] N. Nitta, D. Lei, H. R. Jung, D. Gordon, E. Zhao, G. Gresham, J. Cai, I. Luzinov, G. Yushin, *ACS Appl. Mater. Interfaces* **2016**, *8*, 25991.
[12] W. Liu, H. Xu, H. Qin, Y. Lv, G. Zhu, F. Lin, X. Lei, Z. Zhang, L. Wang, *Silicon* **2019**.
[13] Y. Jin, B. Zhu, Z. Lu, N. Liu, J. Zhu, *Adv. Energy Mater.* **2017**, *7*, 1700715.
[14] Q. Si, D. Mori, Y. Takeda, O. Yamamoto, N. Imanishi, *Energies* **2017**, *10*, 1803.
[15] J. Zhang, C. Zhang, S. Wu, X. Zhang, C. Li, C. Xue, B. Cheng, *Nanoscale Res. Lett.* **2015**, *10*, 395.
[16] C. Wang, H. Wu, Z. Chen, M. T. McDowell, Y. Cui, Z. Bao, *Nat. Chem.* **2013**, *5*, 1042.
[17] K. Feng, M. Li, Y. Zhang, W. Liu, A. G. Kashkooli, X. Xiao, Z. Chen, *Electrochim. Acta* **2019**, *309*, 157.
[18] D. Bresser, D. Buchholz, A. Moretti, A. Varzi, S. Passerini, *Energy Environ. Sci.* **2018**, *11*, 3096.
[19] D. Mazouzi, Z. Karkar, C. Reale Hernandez, P. Jimenez Manero, D. Guyomard, L. Roué, B. Lestriez, *J. Power Sources* **2015**, *280*, 533.
[20] F. Jeschull, D. Brandell, M. Wohlfahrt-Mehrens, M. Memm, *Energy Technol.* **2017**, *5*, 2108.
[21] F. Jeschull, J. Maibach, K. Edström, D. Brandell, *J. Electrochem. Soc.* **2017**, *164*, A1765.
[22] A. Kraytsberg, Y. Ein-Eli, *Adv. Energy Mater.* **2016**, *6*, 1600655.
[23] C. C. Nguyen, B. L. Lucht, *J. Electrochem. Soc.* **2018**, *165*, A2154.
[24] J. L. Gómez-Cámer, C. Bünzli, M. M. Hantel, T. Poux, P. Novák, *Carbon* **2016**, *105*, 42.
[25] B. E. Nilssen, R. A. Kleiv, *Silicon* **2020**.
[26] W. Porcher, B. Lestriez, S. Jouanneau, D. Guyomard, *J. Electrochem. Soc.* **2009**, *156*, A133.
[27] T. Liu, C. Tiu, L. Chen, D. Liu, *Printed Batteries: Materials, Technologies and Applications*, Wiley, New Jersey **2018**.
[28] Z. Karkar, D. Guyomard, L. Roué, B. Lestriez, *Electrochim. Acta* **2017**, *258*, 453.
[29] T. F. Tadros, *Handbook of Colloid and Interface Science*, Vol. *2*, Walter de Gruyter, GmbH, Berlin **2018**.
[30] J. A. Lewis, *J. Am. Ceram. Soc.* **2000**, *83*, 2341.
[31] M. Toivakka, D. Eklund, D. W. Bousfield, *J. Non-Newtonian Fluid Mech.* **1995**, *56*, 49.
[32] P. J. Carreau, P. A. Lavoie, F. Yziquel, *Rheol. Ser.* **1999**, *8*, 1299.
[33] S. Mueller, E. W. Llewellin, H. M. Mader, *Proc. R. Soc. A* **2010**, *466*, 1201.
[34] I. M. Krieger, *Adv. Colloid Interface Sci.* **1972**, *3*, 111.

© 2020 The Authors. Published by WILEY-VCH Verlag GmbH & Co. KGaA, Weinheim